Proceedings of the ASME 2018 37th International Conference on Ocean, Offshore and Arctic Engineering
OMAE2018
June 17-22, 2018, Madrid, Spain

OMAE2018-77676

COMPARISON AND VALIDATION OF HYDRODYNAMIC LOAD MODELS FOR A SEMI-SUBMERSIBLE FLOATING WIND TURBINE

John Marius Hegseth*
Department of Marine Technology
Norwegian University of
Science and Technology
Trondheim, Norway, NO-7491
Email: john.m.hegseth@ntnu.no

Erin E. Bachynski
Department of Marine Technology
Norwegian University of
Science and Technology
Trondheim, Norway, NO-7491
Email: erin.bachynski@ntnu.no

Madjid Karimirad
Civil Engineering Discipline
School of Natural and Built Environment
Queen's University Belfast
Belfast, United Kingdom, BT95AG
Email: madjid.karimirad@qub.ac.uk

ABSTRACT

In global aero-hydro-servo-elastic analyses of floating wind turbines (FWTs), the hydrodynamic loads are usually found from potential flow theory and applied in a single point of a rigid hull. When the hull is relatively stiff, this approach ensures correct behaviour for the six rigid body degrees-of-freedom (DOFs), but provides no information about the internal loads in the hull. The current work considers a simplified method to include distributed, large volume hydrodynamics in the global analysis, where frequency-dependent loads from potential theory are applied on a finite element (FE) model of the hull in a strip-wise manner. The method is compared to conventional load models for a braceless 5MW semi-submersible FWT, and validated against experimental results from model tests with focus on internal loads and rigid body motions in the main wave-frequency range. The global motions are accurately predicted by the distributed model for all investigated load cases. Good agreement with experimental results is also seen for the column base bending moment in wave-only conditions, although extreme values are not captured correctly due to limitations in linear theory. In combined wave-wind conditions, the measured bending moments are significantly increased because of the wind-induced mean angle of the platform. This effect is not considered in the numerical model, which therefore underestimates the moment response. However, an approach which calculates the loads in the actual mean configuration of the hull is found to give reasonably accurate results, at least in moderate wave conditions.

NOMENCLATURE

ξ_j Rigid body motion in mode j
ρ Water density
φ Velocity potential
ω Angular frequency
A_{ij} Added mass matrix entry
B_{ij} Radiation damping matrix entry
C_a Added mass coefficient
COG Center of gravity
DOF Degree of freedom
FE Finite element
FWT Floating wind turbine
H_s Significant wave height
n_i Unit normal vector entry
p_D Diffraction pressure
p_j Radiation pressure in mode j
SWL Still water level
T_p Spectral peak period
U Mean wind speed at hub
VCG Vertical center of gravity
X_i Excitation force vector entry

INTRODUCTION

Hydrodynamic forces on large volume floating structures are usually found from potential flow theory and applied in a single point of a rigid body. One drawback with this method is that internal forces in the hull, which may be important for structural

*Address all correspondence to this author.

design, cannot be calculated in the global analysis. In addition, the flexibility of the floater may affect the dynamic response of the system, especially as turbines increase in size. An alternative is to apply distributed loads from Morison's equation on a beam model, however, though it may give reasonable estimates for the global motions of large volume FWTs [1], the approach is only strictly valid for slender structures. Recently, several studies have looked at the possibility of including hull flexibility while still using large volume hydrodynamics in global analyses of FWTs. Svendsen [2] used a sectional approach to distribute hydrodynamic loads from linear potential theory over a beam model of the hull. A similar method was presented by Luan et al. [3], where sectional loads were derived and compared to the results from a frequency-domain model. The method was later validated against model tests for moderate wave conditions in Luan et al. [4]. Borg et al. [5] utilized a modal approach which took into account interaction effects between deformations in the structure and the surrounding flow, using an iteration scheme to find the added mass for an elastic eigenmode. The approach was further explored by Borg et al. [6], where it was used to derive sectional loads within the substructure. The present work examines the technique presented in [2], and compares it to convential hydrodynamic load models for a 5MW braceless semi-submersible FWT at a water depth of 200 m. Further, the numerical models are validated against model tests performed in the ocean basin facilities of SINTEF Ocean in 2015. The model tests were performed with a scale of 1:30 and included, in addition to waves, wind forces from computer simulations using a real-time hybrid modelling approach. The test methodology and experimental results are described in [7, 8]. A numerical model was calibrated against the experimental results by Berthelsen et al. [9], using measured aerodynamic forces at hub height in the simulations. An extension was presented by Karimirad et al. [10], which included wind forces from blade element/momentum (BEM) theory, as well as second order hydrodynamic loads. The current work considers response in the main wave-frequency range, with focus on global motions and internal loads in the hull.

SYSTEM DESCRIPTION

The braceless CSC semi-submersible consists of a central column connected to three side columns by rectangular pontoons, with main dimensions as given in Tab. 1. The NREL 5MW turbine [11] is used together with the OC3-Hywind tower [12], which is cantilevered to the top of the central column. The hub height is 90 m above still water level (SWL). A catenary mooring system, described in Tabs. 3 and 4, consisting of three lines connected to the end of each pontoon is used for station keeping. In the numerical models, the anchors are slightly moved from their specified position to give a better comparison with the measured pretension in the mooring lines. The pretension is found to be very sensitive to changes in the position of the fairleads and anchors, and the initial inaccuracies may therefore be explained by small errors in the experimental set-up [9]. Measured and modelled mass characteristics of the complete model excluding mooring lines are listed in Tab. 2. As the initial decay tests showed some discrepancies in the pitch and roll natural periods, the vertical center of gravity (VCG) is lowered by 10 % in the numerical models to get a better match with the experimental results, as discussed by Berthelsen et al. [9]. In addition, the moment of inertia (I_{yy}) is lowered by 5 %.

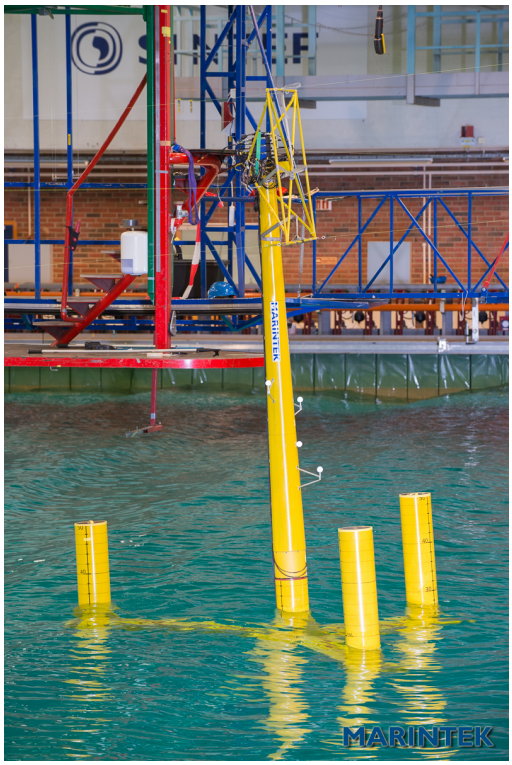

FIGURE 1. VIEW OF THE PHYSICAL MODEL.

The global Earth-fixed coordinate system used in this work, as well as the applied wind and wave directions, are shown in Fig. 2. The origin is located at the SWL, with the z-axis pointing upwards. During the model tests, strain gauges were used to measure the bending moments at the base of side column 3, at a depth of 27 m below SWL. Bending moments were measured about both the x- and y-axis in the body-fixed coordinate system, which coincides with the global coordinate system (both origin and orientation) when the platform is in its static position.

NUMERICAL MODEL

The aero-hydro-servo-elastic analyses are carried out in the time domain, using the simulation workbench SIMA developed by SINTEF Ocean. SIMA couples two computer codes: Riflex, a nonlinear FE tool used to model flexible marine structures; and

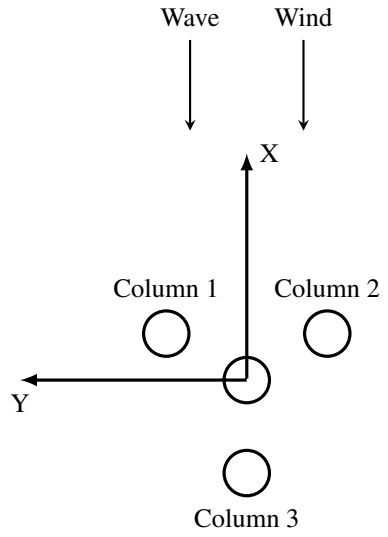

FIGURE 2. SYSTEM LAYOUT.

TABLE 1. OVERALL FULL-SCALE PLATFORM DIMENSIONS.

Parameter	Value
Draft with mooring lines	30.0 m
Column diameter	6.5 m
Pontoon height, width	6 m, 9 m
Central column freeboard	10.0 m
Side column freeboard	20.0 m
Center-to-center distance (central to side column)	41.0 m
Center-to-edge distance (central column to pontoon end)	45.5 m

SIMO, which calculates large volume hydrodynamic loads on rigid bodies [13,14]. The aerodynamic loads are calculated using BEM theory, which includes Glauert correction, Prandtl hub and tip loss factors, dynamic stall, dynamic wake, skewed inflow and tower shadow [15]. An internal control system is used to modify generator torque and blade pitch during the simulations.

The tower is modelled using flexible beam elements, to match as closely as possible the experimental set-up. Bar elements with only axial stiffness are used to model the mooring lines, together with hydrodynamic loads from Morison's equation. As in the model tests, the platform hull and wind turbine blades are considered rigid.

TABLE 2. FULL-SCALE MEASURED AND MODELLED MASS CHARACTERISTICS OF COMPLETE MODEL.

Parameter	Measured value	Modelled value
Mass	9730 tonnes	9730 tonnes
VCG	-19.05 m	-19.95 m
I_{yy} about COG	1.03E+7 tonne $\cdot$ m^2	0.98E+7 tonne $\cdot$ m^2
I_{zz} about COG	7.64E+6 tonne $\cdot$ m^2	7.64E+6 tonne $\cdot$ m^2

TABLE 3. MOORING SYSTEM LAYOUT (FULL-SCALE).

Parameter	Measured value	Modelled value
Fairlead radius	45.95 m	45.95 m
Anchor radius	603.00 m	604.15 m

TABLE 4. FULL-SCALE MOORING LINE CHARACTERISTICS.

Parameter	Segment 1 (upper)	Segment 2 (lower)
Length	240.00 m	367.55 m
Mass density	235.0 kg/m	446.0 kg/m
Wet weight	2.005 kN/m	3.804 kN/m
Equivalent diameter	0.195 m	0.269 m
Axial stiffness	1.88E+8 kN	3.58E+8 kN

HYDRODYNAMIC LOAD MODELS

Three different models for the hydrodynamic loads on the platform are considered in the present work:

1. Single-point potential theory, where the loads are found from linear potential theory and applied in a single point in the hull.
2. Distributed potential theory, where the loads are found from linear potential theory and distributed over the hull using a sectional approach.
3. Morison's equation, where the loads are calculated entirely from Morison's equation.

The models are further described in the following subsections.

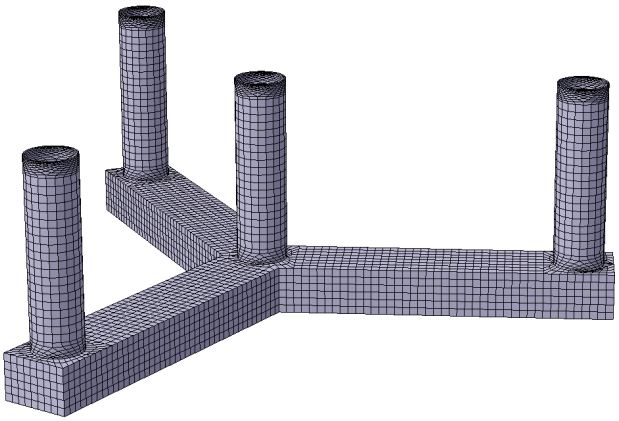

FIGURE 3. PANEL MODEL USED IN THE DIFFRACTION-RADIATION ANALYSIS. 7318 PANELS IN TOTAL.

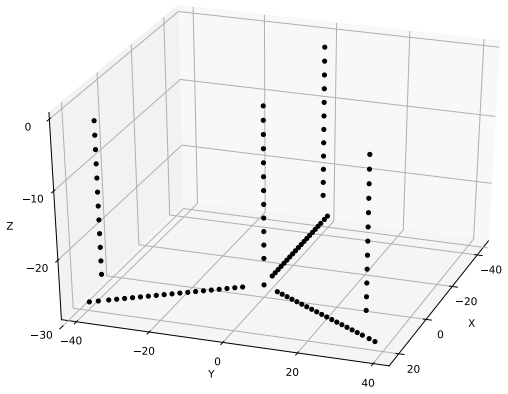

FIGURE 4. BEAM NODES WITH LUMPED HYDRODYNAMIC LOADS.

Single-point potential theory

For the potential theory models, a linear diffraction-radiation analysis is performed in WAMIT [16] to obtain frequency-dependent wave excitation forces, added mass and radiation damping coefficients. The focus of the study is on responses in the main wave-frequency range, and consequently only first order hydrodynamic loads are considered. The velocity potential is found by solving the linearized boundary value problem numerically, where the mean wetted surface of the body is discretized into panels as shown in Fig. 3.

The total velocity potential for a given frequency can be written as a sum of the diffraction potential, φ_D, which includes both the incident and scattering potential, and the radiation potential for each DOF, φ_j:

$$\varphi = \varphi_D + i\omega \sum_{j=1}^{6} \xi_j \varphi_j. \tag{1}$$

The pressure is calculated from the velocity potential using the following relation:

$$p = -\rho \frac{\partial \varphi}{\partial t}. \tag{2}$$

The excitation forces (X_i) and radiation coefficients (A_{ij} and B_{ij}) are then found by integrating the diffraction and radiation pressures, respectively, over the surface of the body:

$$X_i = \iint_{S_b} n_i p_D \, \mathrm{d}S \tag{3}$$

$$A_{ij} - \frac{i}{\omega} B_{ij} = \frac{1}{\omega^2 \xi_j} \iint_{S_b} n_i p_j \, \mathrm{d}S. \tag{4}$$

The resulting hydrodynamic loads are applied in the six rigid DOFs at the hull node, which ensures correct global motions for a stiff hull.

Distributed potential theory

In the distributed model, the hull is divided into sections, which can be considered as individual six DOF bodies. Hydrodynamic loads for each body are then found by integrating the diffraction and radiation pressures over the wetted area of the section. As the initial radiation-diffraction analysis is performed on the complete hull, the sectional loads include hydrodynamic interaction between the structural parts. The bodies are attached to selected nodes in a beam element model, which represents the structural stiffness of the hull. In the current work, a section length of 2 m is used, and the stiffness of the beam elements is set artificially high to represent the rigid hull. An illustration of nodes with applied hydrodynamic loads are shown in Fig. 4.

When the complete hull rotates about the global origin, the motion of an individual section can be described as a combination of a translation and a rotation about its own origin. The resulting pressure on the section reported by WAMIT will therefore consist of both a translational and a rotational part. However, as each section is treated as an individual body, only the latter should be included for the rotational DOFs. The reported rotational pressures can therefore not be used directly in the calculation of sectional loads, as they also contain terms related to translations of the body. Due to this, a simplification is made in that local rotations of the sections are neglected, and only the translational modes are included in the pressure integration. This is illustrated in Fig. 5. The external load vector for each body thus

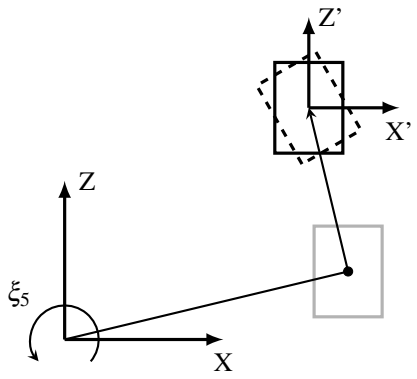

FIGURE 5. TRUE (DASHED) AND APPROXIMATED (SOLID) RIGID BODY DISPLACEMENT USED IN CALCULATION OF SECTIONAL LOADS.

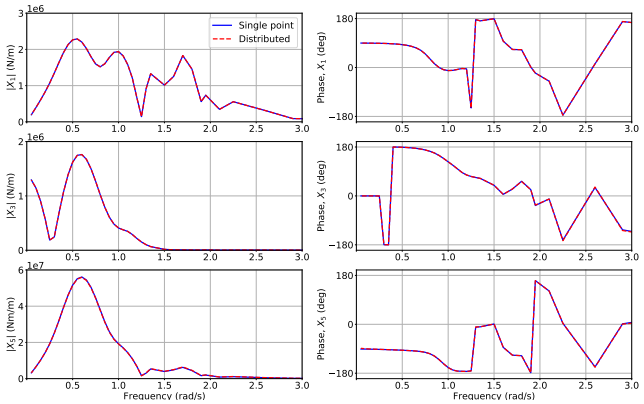

FIGURE 6. EXCITATION FORCES AND MOMENTS, ZERO DEGREE WAVE HEADING, SEGMENT LENGTH 2 m.

only contains the excitation forces in surge, sway and heave, and the radiation coefficients are 3x3 matrices. As a result, the hydrodynamic loads for rotational and coupled rotational-translational modes will only be included in an approximate manner. The global pitch excitation moment on the hull, for instance, will be given as a combination of excitation forces in surge and heave on the individual sections,

$$X_5 \approx \sum_{i=1}^{N} X_{1,i} z_i - X_{3,i} x_i, \tag{5}$$

and similarly for the radiation forces. Due to this approximation, some inaccuracies may be present in the load distribution. The excitation moments approach the exact value when the number of sections increases, but the rotational and translation-rotation terms of the radiation coefficient matrices will not necessarily become more exact.

The accuracy of the distributed model is assessed by comparing summed section forces in surge, heave and pitch with resultant forces reported by WAMIT, presented in Figs. 6 and 7. The total excitation in pitch shows very good agreement for the applied segment length, however, some inaccuracies are present in the radiation coefficients. The added mass is reasonably well approximated, with an error of at most 9 % which occurs in coupled surge-pitch. Larger discrepancies are seen in the damping coefficients, both for B_{55} and B_{51}, especially for frequencies between 0.5 and 1.5 rad/s. Different trends are observed for the coefficients in this frequency range, as the effects of neglecting local rotations vary significantly due to interactions between the different parts of the hull. The importance of these errors on the response of the system is dependent on structural properties such as natural periods and the amount of additional damping, and will therefore vary for different platform designs. As the inaccuracies

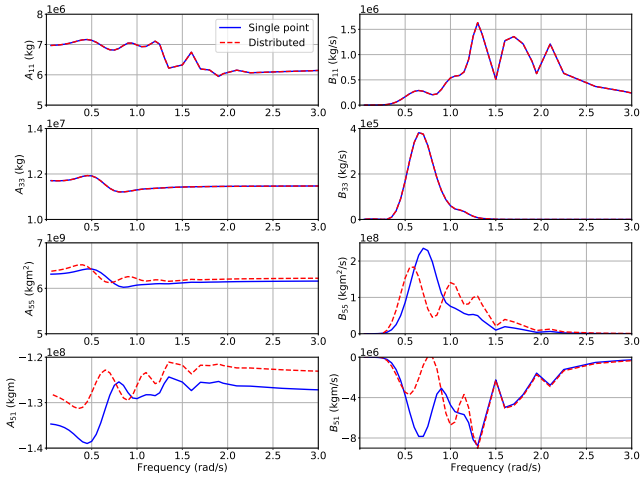

FIGURE 7. ADDED MASS AND RADIATION DAMPING COEFFICIENTS, SEGMENT LENGTH 2 m.

in radiation damping occur at frequencies far away from the natural periods of the 5MW CSC platform, they are not expected to result in notable differences in motion response.

Although not employed in this work, the sectional modelling technique also allows for the hull to be flexible, which may affect the global response for relatively slender hulls. It may also be applied on arbitrary geometries, assuming that the stiffness can be accurately described using beam elements. However, the hydrodynamic boundary value problem is solved with the assumption that the body is rigid. Thus, the effect of hydroelasticity is not fully accounted for, and the method may therefore not be applicable for highly flexible structures.

TABLE 5. APPLIED ADDED MASS COEFFICENTS FOR THE MORISON MODEL.

Structural part	C_a [-]
Columns	1.0
Pontoons (vertical)	1.43
Pontoons (horizontal)	1.64

Morison's equation

The Morison model consists entirely of beam elements with hydrodynamic loads calculated from Morison's equation. As the formulation uses a slender-body approximation to simplify the loads, it is only valid when the diameter to wave length ratio is small. In the current implementation, wave kinematics are calculated up to the instantaneous free surface using the Wheeler stretching method, as this has been found to improve the results for similar structures [1]. Non-dimensional added mass coefficients, listed in Tab. 5, are taken from DNV-RP-H103 [17]. The values compare well to effective added mass coefficients derived from the numerical diffraction-radiation analysis, however, some differences are present due to end effects. Double-symmetric cross sections are used for the pontoons to allow for different coefficients in the vertical and horizontal direction.

Viscous effects are accounted for in all three models using the quadratic drag term from Morison's equation. Berthelsen et al. [9] showed that calibration of the drag coefficients was needed in order to achieve good agreement between measured and calculated low-frequency response. However, viscous forces are of less importance in the wave-frequency range, and such tuning is thus not performed in the current work. The drag coefficients applied on all numerical models are identical to the combined values used in [9].

LOAD CASES

The environmental conditions considered in the current work are summarized in Tab. 6. In the pink noise test, the model was subjected to irregular waves generated from a spectrum nearly constant over a range of frequencies, and zero outside. For the other tests, JONSWAP spectra were used as basis. The wave elevation used in the numerical simulations is equal to the undisturbed wave measured at the global origin without the model present (during wave calibration). TurbSim [18] with the normal turbulence model for class B wind turbines, together with a Kaimal wind spectrum and no vertical wind shear, was used to calculate the turbulent wind time series in test 4310. The applied wind field is identical to the one used in the corresponding hybrid model test. All load cases have a full-scale duration of three hours after removal of transients.

TABLE 6. DESCRIPTION OF SELECTED MODEL TESTS.

Test no.	H_s [m]	T_p [s]	U [m/s]	Comment
2321	4.0	4.5-22	-	Pink noise
2420	3.6	10.2	-	Moderate wave
2410	15.3	14.0	-	50-year storm wave
4310	3.6	10.2	11.0	Same wave as 2420, near rated wind speed

RESULTS

Decay tests

Natural periods for the rigid body motions of the system were found from decay analyses in calm water and are listed in Tab. 7. There is good agreement between the numerical models, and also with the experimental results. Deviations in the rotational modes can be explained by inaccurate representation of the added mass in the distributed and Morison models.

TABLE 7. NATURAL PERIODS FOUND FROM DECAY TESTS.

Mode	Experiment	Rigid	Distributed	Morison
Surge (s)	86.5	85.0	84.9	85.3
Sway (s)	86.5	85.0	85.1	85.3
Heave (s)	25.3	25.4	25.4	25.0
Roll (s)	29.8	30.0	31.0	31.2
Pitch (s)	29.7	30.0	31.0	31.2
Yaw (s)	61.7	61.4	58.8	65.1

Response amplitude operators

Results from the pink noise test are used to calculate response amplitude operators (RAOs) for global motions and column bending moment, which was shown by Bachynski et al. [8] to be consistent with RAOs derived from regular wave tests with 1/60 steepness for the 5MW CSC platform. There is good agreement between numerical and experimental results for the global motions, presented in Fig. 8. Some deviations between the models are seen at lower frequencies in pitch, likely caused by differences in radiation damping, which becomes more important as the response approaches the natural frequency.

As shown in Fig. 9, the distributed potential theory model also gives accurate estimates for the column bending moment,

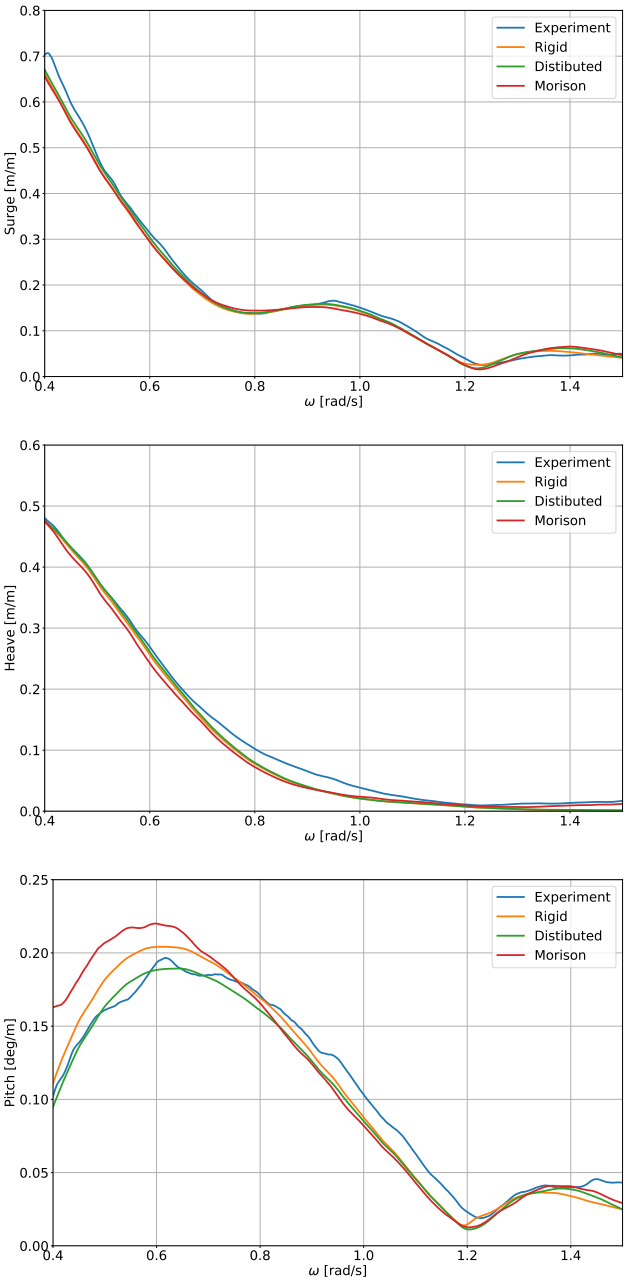

FIGURE 8. MOTION RAOs FROM PINK NOISE, TEST 2321.

while Morison's equation, as expected, overestimates the loads at higher frequencies where diffraction effects become important. Deviation from potential theory is visible from approximately 0.9 rad/s, which corresponds to a diameter to wavelength ratio of about 0.1 for the column.

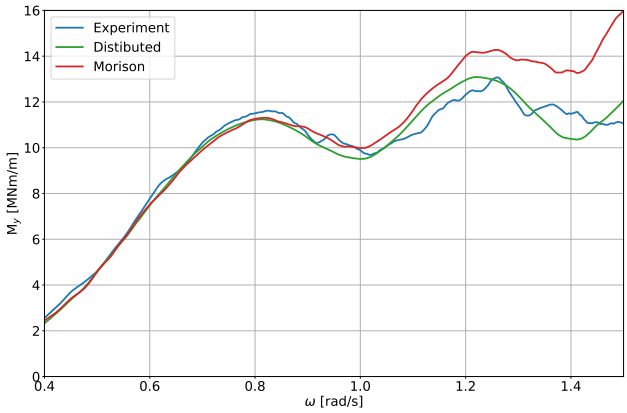

FIGURE 9. COLUMN MOMENT RAO FROM PINK NOISE, TEST 2321.

Bending moments in moderate and extreme waves

In addition to the pink noise test, two analyses with irregular waves and no aerodynamic loading are used to study the internal load response in wave-only conditions. Figure 10 compares bending moment spectra for the column in moderate waves (test 2420). Both numerical models agree well with experimental results, as the wave spectrum has a very limited amount of energy at higher frequencies where Morison's equation becomes less valid. From the column moment statistics in Fig. 11, the standard deviation is seen to vary little between the models, while the maximum and minimum values are slightly underestimated by distributed potential theory. The main reason for this is believed to be that the wave loads only are integrated up to the mean free surface in linear theory.

This approximation becomes less accurate when the wave severity increases, as shown in Figs. 12 and 13 for the 50-year storm condition. The standard deviation is still quite accurately estimated, however, the maximum bending moment is now only 30 % of the experimental value. A distributed potential theory model where forces up to the instantaneous free surface are included using a simplified approach, is also studied. Here, Morison loading is applied only on the column elements above SWL, and the wave kinematics are stretched. Although this gives a closer match around the spectral peak frequency, the maximum bending moment is still only 65 % of the measured value, and the modified model is also seen to overestimate the response at higher frequencies.

As seen in Fig. 13, the numerical models in general fail to capture the large asymmetry in the measured extreme loads, where the absolute value of the positive extreme bending moment is about 2.5 times larger than the negative one. The results suggest that higher order wave kinematics, which become increasingly important as the wave height increases, also must be considered in order to accurately predict extreme values for the

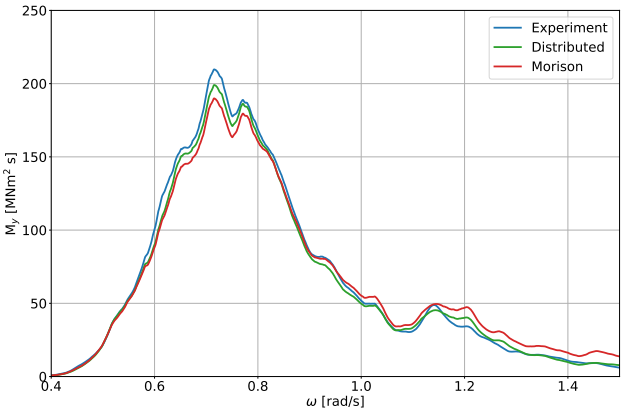

FIGURE 10. COLUMN MOMENT SPECTRAL DENSITY IN MODERATE WAVES, TEST 2420.

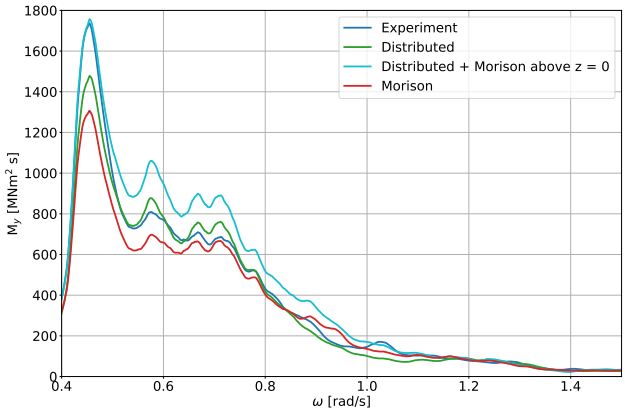

FIGURE 12. COLUMN MOMENT SPECTRAL DENSITY IN EXTREME WAVES, TEST 2410.

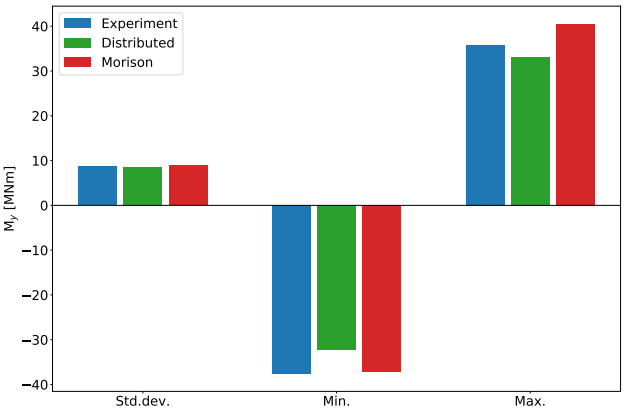

FIGURE 11. COLUMN MOMENT STATISTICS IN MODERATE WAVES, TEST 2420.

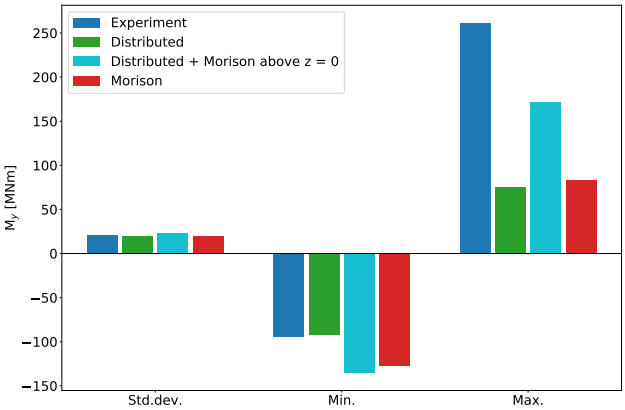

FIGURE 13. COLUMN MOMENT STATISTICS IN EXTREME WAVES, TEST 2410.

internal loads.

Response in irregular waves and turbulent wind

Finally, the system is analysed with irregular waves and turbulent wind near rated wind speed, which gives the maximum thrust force on the turbine. Figure 14 shows that there is good agreement between the potential theory models and experimental values for the wave-frequency motion response. The Morison model, on the other hand, fails to accurately describe the rigid body motions of the platform, where especially the pitch response is poorly estimated.

The inclusion of wind is seen to have a large impact on the column bending moment, also in the wave-frequency range, as the values in Figs. 15 and 16 are significantly increased compared to the wave-only condition with identical waves (test 2420). This is mainly caused by a change in column geometry relative to the waves, due to the wind-induced mean pitch angle of the platform. The mean pitch angle in the current wind conditions is 5.8°, which results in an increased submerged length of approximately 4 m for the column.

As the Morison model calculates hydrodynamic forces in the instantaneous position of the hull, this effect is captured in the simulation. The column bending moment is mainly dependent on wave excitation forces, and Morison's equation is therefore able to quite accurately predict the moment response for lower frequencies, where the slender-body approximation is more valid, despite the errors in global motions.

The distributed potential theory model, on the other hand, does not take into consideration the updated configuration of the hull, and consequently underestimates the bending moments. In order to improve the accuracy of the model, the diffraction-radiation analysis is rerun on a modified panel model, which

considers the submerged volume of the hull when given a rotation equal to the mean pitch angle from the simulation. The sectional hydrodynamic loads are then updated, and the dynamic analysis is performed as before. This does not affect the global motions of the platform (not shown), but clearly improves the internal load response, and the bending moment standard deviation is within 10 % of the experimental value. The bending moments are still somewhat underestimated, which likely is related to the limitations in linear theory discussed in the previous section.

The mean pitch angle of the platform for a given environmental condition, which is needed for the updated hydrodynamic analysis, is in general not known a priori. However, it can be found from an initial simulation, or estimated from the wind turbine thrust curve and the pitch restoring of the system.

CONCLUSIONS

A simple approach for including distributed hydrodynamic loads on large volume structures are compared to conventional load models, and a validation against hybrid model tests is performed with regards to global motions and internal loads for a 5MW braceless semi-submersible FWT. Due to simplifications made in the pressure integration for the distributed potential theory model, some errors are seen in the total added mass and damping coefficients. However, this is found to have very limited influence on the motion response for the current platform design, and the global motions are accurately estimated by the distributed model for all investigated load cases. Good agreement with experimental results is also seen for the column bending moment in wave-only conditions, although maximum values are significantly underestimated in storm waves due to limitations in linear theory. The results suggest that higher-order wave kinematics are needed in order to capture the extreme bending moments.

In combined wave-wind conditions, the wind-induced mean angle of the platform may be important for the internal load response in members far from the rotational axis, as relatively small angles can lead to large differences in the submerged geometry and thus the hydrodynamic loads. This effect is not considered in the potential theory model, which calculates the loads based on the static position of the hull before any environmental loads are applied, and consequently underestimates the moment response. However, a potential theory approach which considers the actual mean configuration of the platform performs reasonably well, at least in moderate wave conditions. The numerical model with pure Morison loading calculates the hydrodynamic loads in the instantaneous position of the structure, and is able to accurately predict the moment response up to a frequency of about 0.9 rad/s. For higher frequencies the bending moment is overestimated, as diffraction effects become important.

The present work is performed for a rigid hull, and structural deformations are thus not considered. However, the distributed potential theory approach may also be used to study the effect of hull flexibility, at least for structures where hydroelasticity effects are not important. Future studies should therefore consider a floater with more realistic stiffness, in order to validate the method for deformable bodies.

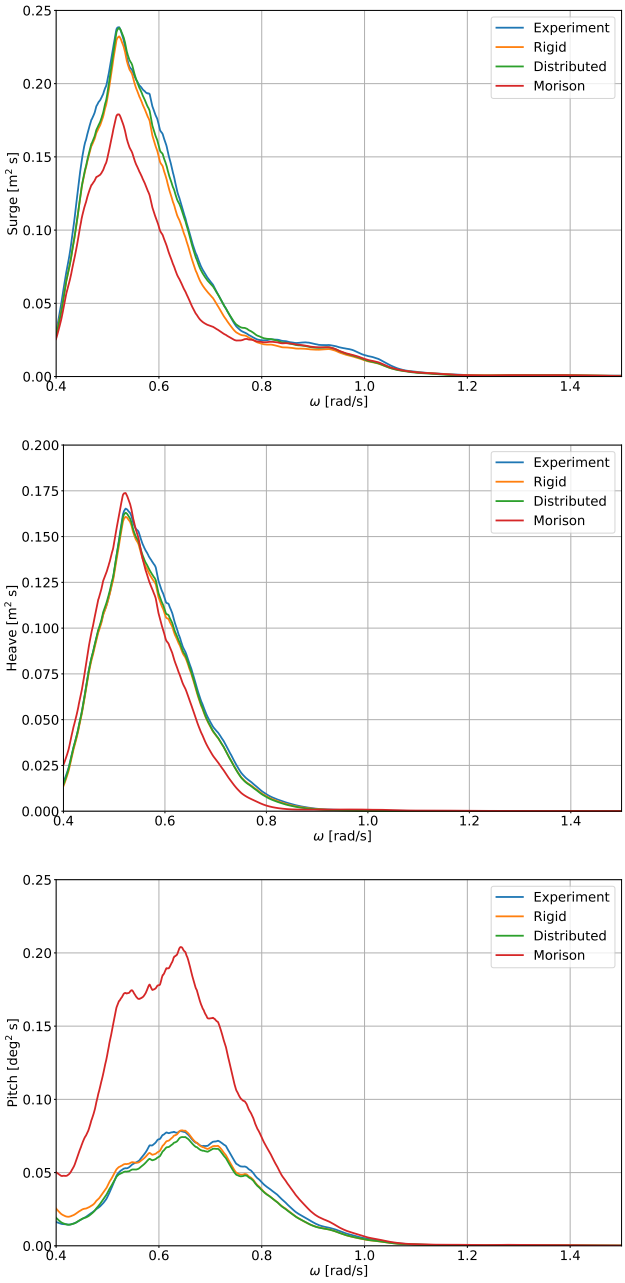

FIGURE 14. SURGE, HEAVE AND PITCH SPECTRAL DENSITY IN MODERATE WAVES AND RATED WIND SPEED, TEST 4310.

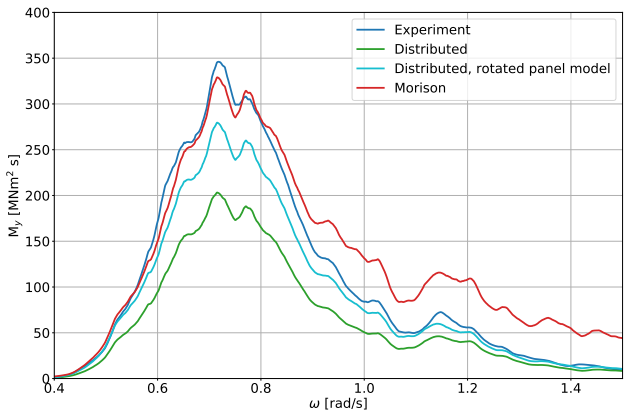

FIGURE 15. COLUMN MOMENT SPECTRAL DENSITY IN MODERATE WAVES AND RATED WIND SPEED, TEST 4310.

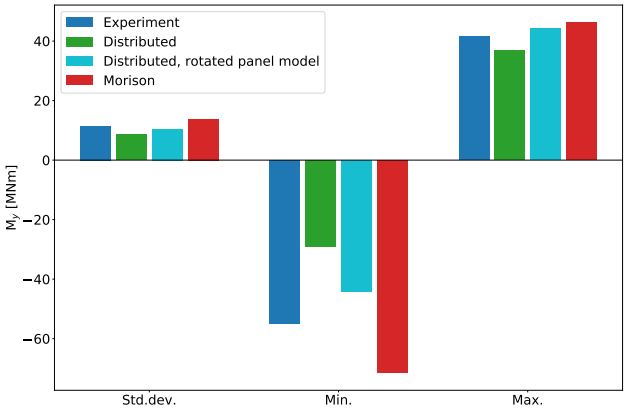

FIGURE 16. COLUMN MOMENT STATISTICS IN MODERATE WAVES AND RATED WIND SPEED, TEST 4310.

ACKNOWLEDGMENT

The authors acknowledge Norwegian Research Centre for Offshore Wind Technology (NOWITECH), NFR project 193823.

REFERENCES

[1] Kvittem, M. I., Bachynski, E. E., and Moan, T., 2012. "Effects of Hydrodynamic Modelling in Fully Coupled Simulations of a Semi-Submersible Wind Turbine". *Energy Procedia,* ***24***, pp. 351–362.

[2] Svendsen, K. F., 2016. "Structural Design and Dynamic Analysis of a Tension Leg Platform Wind Turbine , Considering Elasticity in the Hull". Master's thesis, Norwegian University of Science and Technology.

[3] Luan, C., Gao, Z., and Moan, T., 2017. "Development and Verification of a Time-Domain Approach for Determining Forces and Moments in Structural Components of Floaters with an Application to Floating Wind Turbines". *Marine Structures,* ***51***, pp. 87–109.

[4] Luan, C., Chabaud, V., Bachynski, E. E., Gao, Z., and Moan, T., 2017. "Experimental Validation of a Time-Domain Approach for Determining Sectional Loads in a Floating Wind Turbine Hull Subjected to Moderate Waves". In Proceedings of the 14th Deep Sea Offshore Wind R&D Conference, EERA DeepWind'2017, Trondheim, Norway.

[5] Borg, M., Hansen, A. M., and Bredmose, H., 2016. "Floating Substructure Flexibility of Large-Volume 10MW Offshore Wind Turbine Platforms in Dynamic Calculations". *Journal of Physics: Conference Series,* ***753***(8), p. 082024.

[6] Borg, M., Bredmose, H., and Hansen, A. M., 2017. "Elastic Deformations of Floaters for Offshore Wind Turbines: Dynamic Modelling and Sectional Load Calculations". In Proceedings of the ASME 2017 36th International Conference on Ocean, Offshore and Arctic Engineering (OMAE2017), Trondheim, Norway.

[7] Sauder, T., Chabaud, V., Thys, M., Bachynski, E. E., and Sæther, L. O., 2016. "Real-Time Hybrid Model Tests of a Braceless Semi-Submersible Wind Turbine. Part I: The Hybrid Approach". In Proceedings of the ASME 2016 35th International Conference on Ocean, Offshore and Arctic Engineering (OMAE2016), Busan, South Korea.

[8] Bachynski, E. E., Thys, M., Sauder, T., Chabaud, V., and Sæther, L. O., 2016. "Real-Time Hybrid Model Tests of a Braceless Semi-Submersible Wind Turbine. Part II: Experimental Results". In Proceedings of the ASME 2016 35th International Conference on Ocean, Offshore and Arctic Engineering (OMAE2016), Busan, South Korea.

[9] Berthelsen, P. A., Bachynski, E. E., Karimirad, M., and Thys, M., 2016. "Real-Time Hybrid Model Tests of a Braceless Semi-Submersible Wind Turbine. Part III: Calibration of a Numerical Model". In Proceedings of the ASME 2016 35th International Conference on Ocean, Offshore and Arctic Engineering (OMAE2016), Busan, South Korea.

[10] Karimirad, M., Bachynski, E. E., Berthelsen, P. A., and Ormberg, H., 2017. "Comparison of Real-Time Hybrid Model Testing of a Braceless Semisubmersible Wind Turbine and Numerical Simulations". In Proceedings of the ASME 2017 36th International Conference on Ocean, Offshore and Arctic Engineering (OMAE2017), Trondheim, Norway.

[11] Jonkman, J., Butterfield, S., Musial, W., and Scott, G., 2009. Definition of a 5-MW Reference Wind Turbine for Offshore System Development. Tech. Rep. NREL/TP-500-38060, National Renewable Energy Laboratory.

[12] Jonkman, J., 2010. Definition of the Floating System for Phase IV of OC3. Tech. Rep. NREL/TP-500-47535, Na-

tional Renewable Energy Laboratory.
[13] MARINTEK, 2016. RIFLEX User Guide.
[14] MARINTEK, 2016. SIMO User Guide.
[15] Ormberg, H., and Bachynski, E. E., 2012. "Global Analysis of Floating Wind Turbines: Code Development, Model Sensitivity and Benchmark Study". In Proceedings of the Twenty-second (2012) International Offshore and Polar Engineering Conference (ISOPE2012), Rhodes, Greece.
[16] Wamit Inc ., 2014. WAMIT User Manual.
[17] DNV, 2011. Modelling and Analysis of Marine Operations. Tech. Rep. DNV-RP-H103.
[18] Jonkman, B. J., 2009. TurbSim User's Guide: Version 1.50. Tech. Rep. NREL/TP-500-46198, National Renewable Energy Laboratory.